DOI: 10.1002/((please add manuscript number))

Article type: Full Paper

Improved Efficiency and Stability of Pb/Sn Binary Perovskite Solar Cells Fabricated by Galvanic Displacement Reaction

Zonglong Zhu,[1,2†] Nan Li,[1,3†] Dongbin Zhao,[1,4] Liduo Wang,[3] and Alex K.-Y. Jen[1,2,5*]

Dr. Z. Zhu, Dr. N. Li, Dr. D. Zhao, Prof. A. K.-Y. Jen

[1]Department of Materials Science & Engineering, University of Washington, Seattle, Washington, 98195, United States

Dr. Z. Zhu, Prof. A. K.-Y. Jen

[2]Department of Chemistry, City University of Hong Kong, Kowloon, Hong Kong

Dr. N. Li, Pro. L. Wang

[3]Key Lab of Organic Optoelectronics & Molecular Engineering of Ministry of Education, Department of Chemistry, Tsinghua University, Beijing 100084, China

Dr. D. Zhao,

[4]State Key Laboratory and Institute of Elemento-Organic Chemistry, Collaborative Innovation Center of Chemical Science and Engineering, Nankai University, Tianjin 300071, China

Prof. A. K.-Y. Jen

[5]Department of Materials Science and Engineering, City University of Hong Kong, Kowloon, Hong Kong

Keyword: Galvanic Displacement Reaction, Pb/Sn Binary Perovskite, Solar Cells

†These authors contributed to this work equally.

*Corresponding author. E-mail: alexjen@cityu.edu.hk

Abstract

Although the field of tunable bandgap Pb-Sn binary perovskites (from 1.17 to 1.55 eV) has seen dramatic progress in device efficiency, the long-term stability of perovskites and their derived devices still needs to be improved due to the easy oxidation of Sn^{2+} to Sn^{4+}. Here we demonstrate a simple and generally applicable method of fabricating efficient and stable Pb-Sn binary perovskite solar cells (PVSCs) based on a galvanic displacement reaction (GDR). Different from the commonly used conventional approaches to form perovskite precursor solutions by mixing metal halides and organic halides such as PbI_2, SnI_2, MAI, FAI, etc. together, our precursor solutions were formulated by reacting pure Pb-based perovskite precursor solutions with fine Sn metal powders. After the ratios between Pb and Sn were optimized, high PCEs of 15.85% and 18.21% could be achieved for $MAPb_{0.4}Sn_{0.6}I_3$ and $(FAPb_{0.6}Sn_{0.4}I_3)_{0.85}(MAPb_{0.6}Sn_{0.4}Br_3)_{0.15}$ based PVSCs, which are the highest PCEs among all values reported to date for Pb-Sn binary PVSCs. Moreover, the GDR perovskite based PVSCs exhibit significantly improved ambient and thermal stability with encapsulation, which can retain more than 90% of their initial PCEs after being stored in ambient (RH~50%) for 1000 h or being thermal annealed at 80 °C for more than 120 h in ambient. Our results demonstrate the great advantage of using GDR to prepare tunable bandgap binary perovskites for devices with greatly improved performance and stability.

Introduction

Organic-inorganic hybrid perovskite solar cells (PVSCs) have attracted worldwide attentions as one of very promising printable solar cell systems for renewable engery.[1-4] Under only a very short period of development, a certified power conversion efficiency (PCE) of 23.3% has been demonstrated,[5] which can rival the performance of the existing inorganic photovoltaic technologies. Recently, Pb-Sn binary perovskites show great promise for the development of ideal bandgap (1.3-1.4 eV) solar cells due to the relative ease in tuning their bandgap (E_g) compared to the parent Pb-based counterpart. By tuning the ratios of Pb-Sn, we and others have demonstrated that the E_g of Pb-Sn perovskites can be easily manipulated with the lowest value achieved at around 1.2 eV,[6, 7] leading to a PCE of >17% in the resulting PVSC.[8-13] Such advancement has facilitated the building of tandem cells using Pb-Sn based PVSC with a 18.5% PCE in a monolithic two-terminal tandem and a PCE of 20.3% in a mechanically stacked tandem.[9, 14]

In spite of demonstrated high efficiencies, the reliability of the binary Pb-Sn PVSCs is still a serious problem that needs to be addressed. The main reason for the instability is the easy oxidation of Sn^{2+} to Sn^{4+}, which degrades both the semiconducting properties and film quality of binary perovskites.[15-18] To alleviate this deficiency, numerous composition engineering or precursor formulations have been attempted, such as the introduction of reducing additives or 2D organic components into perovskite precursor to suppress Sn^{2+} oxidation.[19, 20] For example, SnF_2 has been used in forming Sn or Pb-Sn binary perovskites to reduce Sn^{2+} oxidation in the solution. However, the existence of SnF_2 additives will adversely impact the film morphology of Sn-containing perovskite films, which is detrimental to the long-term stability of devices.[21-24] The modulation of 3D Sn-based perovskite into 2D/3D layered structures can slow down oxygen permeation to retard Sn^{2+} oxidation,[25, 26] however, the resulting perovskites still suffer from self-oxidation of Sn^{2+} to Sn^0 and Sn^{4+} and the absorbers degrade even under inert environment.

In this work, we report a simple but effective method in fabricating Pb-Sn binary perovskite films by utilizing a galvanic displacement reaction (GDR). Different with the conventional methods that mix PbI_2, SnI_2, MAI, FAI initially to form perovskite precursor solutions, our binary Pb-Sn precursor solutions were formulated by reacting pure Pb perovskite precursor solutions with fine Sn metal powders. Very encouragingly, the PVSC based on the derived $MAPb_{0.4}Sn_{0.6}I_3$ perovskite showed a high current density of 25.51 mA cm^{-2}, leading to a promising PCE of 15.85%. The device efficiency can be further improved by applying this method to prepare a mixed perovskite $(FAPb_{0.6}Sn_{0.4}I_3)_{0.85}(MAPb_{0.6}Sn_{0.4}Br_3)_{0.15}$, which can result in an even higher PCE of 18.21%. This is the highest PCE value among all reported Pb-Sn binary PVSCs. Moreover, the device was found to exhibit very good ambient stability, which could retain >90% of its initial PCE after being stored in ambient (RH~50%) for 1000 h. It can also survive thermal annealing at 80 °C for >300 h in ambient. To understand the mechanism that leads to improved stability, X-ray spectroscopy (XPS) was employed to investigate the chemical states of Sn and Pb in the perovskite. It was found that oxidation of Sn^{2+} to Sn^{4+} can be suppressed in the GDR prepared films. This simple approach can also be applied to make other perovskites and the knowledge gained in understanding device degradation can help guide future development of binary perovskites to achieve longer device lifetime.

Preparation of Pb-Sn based perovskite solution via GDR and the film characterization

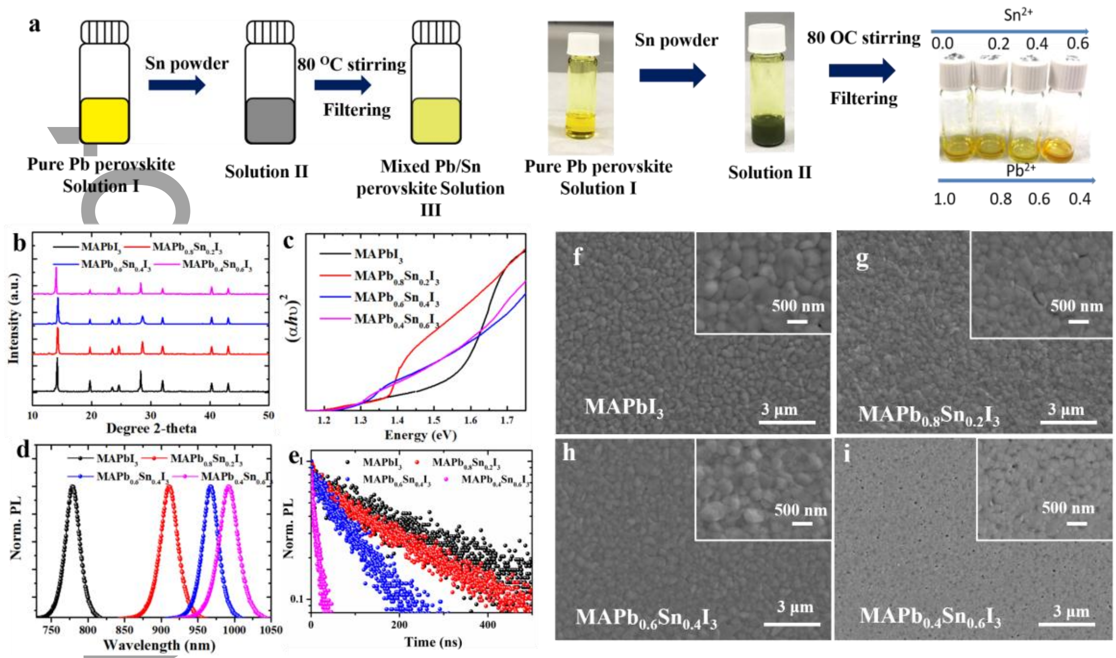

Figure 1 **a**) Schematic drawing and photographs of the $MAPb_xSn_{1\text{-}x}I_3$ solution preparation *via* GDR between $MAPbI_3$ solution and Sn powders; **b**) XRD spectra, **c**) UV-vis spectra, and **d**) steady-state and **e**) time-resolved PL spectra of the studied $MAPb_{1-x}Sn_xI_3$ films fabricated by the perovskite solutions prepared by GDR. The SEM images of the **f**) $MAPbI_3$, **g**) $MAPb_{0.8}Sn_{0.2}I_3$, **h**) $MAPb_{0.6}Sn_{0.4}I_3$, **i**) $MAPb_{0.4}Sn_{0.6}I_3$ films fabricated by the solutions prepared by GDR.

A typical galvanic displacement reaction (GDR)[27] is a redox process occurred between metal and metal ions in solution, driven by the difference between redox potentials.[28-30] Hence, when this method was adopted to prepare binary Pb-Sn precursor solutions, the driving force for the GDR is the difference between the redox potential of Sn^{2+} and Pb^{2+}. The standard redox potentials for the involved materials are given in the following equations (a–c)[31]:

$$Sn^{2+} + 2e^- \rightarrow Sn_{(s)},\ E^{\ominus} = -0.14\,V \quad \text{(a)}$$

$$Sn^{4+} + 2e^- \rightarrow Sn^{2+},\ E^{\ominus} = 0.15\,V \quad \text{(b)}$$

$$Pb^{2+} + 2e^- \rightarrow Pb_s,\ E^{\ominus} = -0.13\,V \quad \text{(c)}$$

Based on the above equations, the final balanced equation in the binary Pb-Sn precursor solution should be:

$$Sn(s) + Pb^{2+} \rightarrow Sn^{2+} + Pb\ (s);\ \ E^{\ominus} = 0.01\ V,\ \Delta G < 0 \quad \text{(d)}$$

Therefore, when the Sn powders were added into the $MAPbI_3$ precursor solution (as depicted in **Figure 1a**), a suspension is formed initially. The Sn atoms on the metal surface were oxidized by the Pb^{2+} ions owing to the GDR while the Pb^{2+} ions were gradually replaced by the Sn^{2+} ions in the precursor solution. Meanwhile, the Pb atoms could be deposited on the Sn metal surface to form Pb/Sn alloy or aggregating together to form Pb nanoparticles. Note that the reaction will keep the tin ions at the Sn^{2+} state because further oxidation of Sn^{2+} to Sn^{4+} needs higher driving force but the electrochemical dynamics between Sn^{2+} and Pb^{2+} lack such driving voltage due to the positive ΔG in the equation shown below:

$$Sn^{2+} + Pb^{2+} \rightarrow Sn^{4+} + 2Pb\ (s)\ E^{\ominus} = -0.02\ V,\ \Delta G > 0 \quad \text{(e)}$$

The GDR was performed by stirring the solution at 80 °C for several hours and the reaction mixture was then filtered to remove the solid Pb products and excessive Sn powders from the solution. The detailed experimental procedures were described in the experiment section. As shown in **Figure 1a**, clear solutions could be obtained after different reacting times in forming the $MAPb_{1-x}Sn_xI_3$ precursor solutions. The clear yellow color of the prepared solutions indicates there was no Sn^{4+} formed during the GDR because the existence of Sn^{4+} will turn the solution into reddish color.[32] Subsequently, these precursor solutions were spin-coated onto PEDOT:PSS hole-transporting layer *via* an anti-solvent dripping process and then annealed at 100 °C to prepare the $MAPb_{1-x}Sn_xI_3$ perovskite thin films, wherein the x ranges from 0, 0.2, 0.4. to 0.6, as confirmed by the XPS analysis (**Table S1**).

Figure 1b showed the X-ray diffraction (XRD) patterns of the studied $MAPb_{1-x}Sn_xI_3$ films. It has been documented that $MASnI_3$ and $MAPbI_3$ possess pseudo cubic (P4mm) α-phase and tetragonal (I4 cm) β-phase crystal structure, respectively, at room temperature (298K).[6] The XRD patterns of these as-prepared $MAPb_{1-x}Sn_xI_3$ films all showed intense characteristic peaks of the perovskite crystal structure. However, these feature peaks gradual decrease as the x increased, indicating the Sn incorporation in the perovskite film would reduce film crystallinity. Notably, the $MAPb_{1-x}Sn_xI_3$ films with x = 0, 0.2, and 0.4 showed two obvious peaks within the 2θ range of 22°-25° corresponding to the (211) and (202) planes in the tetragonal I4cm space group while there is only one peak observed at ~24 ^{o} for the $MAPb_{0.4}Sn_{0.6}I_3$ film.[6] This transition can be attributed to the higher symmetry of the pseudo cubic P4mm space group than the tetragonal I4cm space group.

Shown in **Figure 1c** is the Tauc plots of these $MAPb_{1-x}Sn_xI_3$ films that derived from the UV-vis absorption spectrum from **Figure S1**. As shown, the band edges of these Sn-incorporated films red-shifted compared with the pristine $MAPbI_3$ film. The increase of Sn substitution resulted anomalous bandgap variation with Eg shift which has also been reported previously in the literature.[15] The steady-state and time-resolved photoluminescence (PL) spectroscopy was next conducted to probe the charge dynamics of these $MAPb_{1-x}Sn_xI_3$ films deposited on the glass substrates. As shown in **Figure 1d**, the PL peak of the film gradually red-shifted as x increased, in good agreement with the E_g variation observed in **Figure 1c**. The lowest emission wavelength, corresponding to a bandgap of ∼1.23 eV, was observed for the $MAPb_{0.4}Sn_{0.6}I_3$ film. Presented in **Figure 1e** is the corresponding time-resolved PL spectra measured by exciting the prepared film with a 470nm pulsed laser and the PL decay was fitted by the single-exponential decay model. As shown in **Table S2**, the carrier lifetime was 156 ns, 102 ns, 22 ns for the $MAPb_{0.8}Sn_{0.2}I_3$, $MAPb_{0.6}Sn_{0.4}I_3$, $MAPb_{0.4}Sn_{0.6}I_3$ films, respectively. They are all shorter than the value (203 ns) of the pristine $MAPbI_3$ film, suggesting that the Sn incorporation will unavoidably induce the defect density in the film.

Figure 1f-1i are the scanning electron microscopy (SEM) images of these studied films to show their surface morphology. The related EDS mapping has been shown in **Figure S2**, which demonstrated the Sn concentration increase with Sn power reacted with Pb (II) solution. As can be seen, the surface morphology has a strong correlation with the ratio of Pb/Sn. The pure $MAPbI_3$ film displays a highly dense and compact morphology with a relatively large grain size of ~ 500 nm (**Figure 1f**). After the Sn incorporation in the composition, the crystal domain size becomes smaller to ~ 200 nm for both $MAPb_{0.8}Sn_{0.2}I_3$ and $MAPb_{0.6}Sn_{0.4}I_3$ films but the films still possess a good surface coverage with a highly dense and compact morphology, which is needed for efficient PVSCs. However, as the ratio of Sn increases to 60%, the film starts to show a rough surface accompanied with visible pinholes. This poor surface morphology and coverage could be attributed to the rapid crystallization of Sn-based perovskite, which is generally observed in the Sn-containing perovskite films.[33]

Device performance

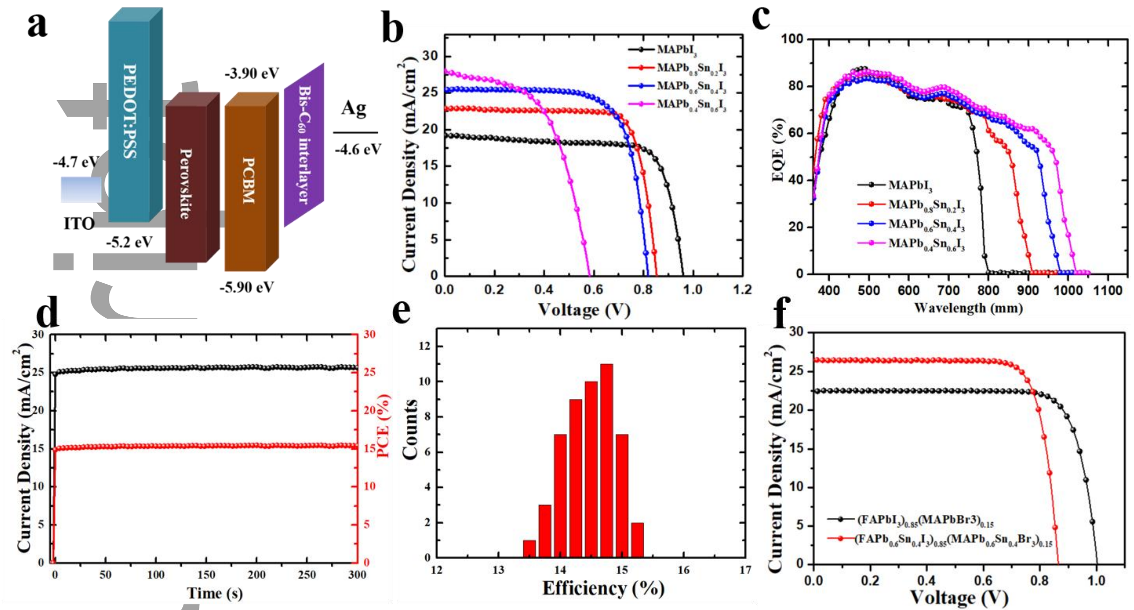

Figure 2 a) Energy diagram of the fabricated PVSC. **b**) Current density-voltage (*J-V*) curves and **c**) related EQE spectrums of the studied PVSCs containing different amount of Sn. **d**) The stable output current and PCE of $MAPb_{0.6}Sn_{0.4}I_3$ PVSC which measured under a constant bias of 0.67 V near the maximum power point. **e**) The PCE distribution statistics of the studied devices. **f**) *J-V* characteristics of the mix-ion PVSC devices with and without Sn content.

To examine the photovoltaic performance of these binary Pb-Sn perovskite films, inverted p-i-n PVSCs with the device configuration of ITO/PEDOT:PSS/$MAPb_{1-x}Sn_xI_3$/PCBM/Bis-C_{60}/Ag were fabricated. The corresponding energy level diagram of the device is illustrated in **Figure 2a**. Their resultant photocurrent-voltage (*J-V*) curves measured under AM 1.5 G irradiation at 100 mW cm^{-2} were compared in **Figure2b** and the related photovoltaic parameters were summarized in **Table S3.** As shown, the control $MAPbI_3$ PVSCs showed a decent PCE of 14.15% with an open-circuit voltage (V_{oc}) of 0.96 V, a short-circuit current density (J_{sc}) of 19.20 mA cm^{-2}, and a fill factor (FF) of 76.8 %. It is noteworthy, the photocurrent was apparently raised for the Sn-containing PVSCs and increased with the Sn-containing ratio due to the anomalous E_g bowing effect as reported in the literature.[6, 34] The J_{sc} for the $MAPb_{0.8}Sn_{0.2}I_3$, $MAPb_{0.6}Sn_{0.4}I_3$ and $MAPb_{0.4}Sn_{0.6}I_3$

PVSCs are 22.87 mA cm^{-2}, 25.51 mA cm^{-2} and 27.94 mA cm^{-2}, respectively. The champion device performance is based on the $MAPb_{0.6}Sn_{0.4}I_3$ composition, which delivered a PCE of 15.76% with a V_{OC} of 0.82 V, a J_{SC} of 25.51 mA cm^{-2}, and a *FF* of 75.60% without showing hysteresis even under a scan rate of 100 mV/s (**Figure S3**).

In addition, the integrated photocurrent extracted from its commensurate external quantum efficiency (EQE) spectrum (**Figure 2c and S4**) matches well with the J_{SC} obtained from the *J-V* curve. These results confirm the high PCE extracted from *J-V* curve. The stabilized photocurrent measured under a bias near the maximum power point of the champion device was shown in **Figure 2d** to confirm the reliability of performance. As shown, a steady J_{sc} of ~25.42 mA cm^{-2} corresponding to a PCE of 15.1% was clearly observed. **Figure 2e** displayed the PCE statistics distribution of total 60 devices of the $MAPb_{0.6}Sn_{0.4}I_3$ PVSC, revealing good reproducibility. Over 90% of the tested devices showed PCE above 14%. To prove the GDR method is a generally applicable strategy to prepare Pb-Sn perovskite solutions, we have applied this method to prepare mixed **$(FAPbI_3)_{0.85}(MAPbBr_3)_{0.15}$** perovskite system and the absorption band edge redshifted to 970 nm (**Figure S5**). Notably, as shown in **Figure 2f**, the devices showed a much higher average PCE of 18.21% in **$(FAPb_{0.6}Sn_{0.4}I_3)_{0.85}(MAPb_{0.6}Sn_{0.4}Br_3)_{0.15}$**-based PVSCs with negligible hysterisis (**Figure S7**), which demonstrated the general applicability of the GDR approach. The charecterizations inculding SEM, XRD, PL, Time-resolved PL and XPS of the studied **$(FAPb_{0.6}Sn_{0.4}I_3)_{0.85}(MAPb_{0.6}Sn_{0.4}Br_3)_{0.15}$** films fabricated by the perovskite solutions prepared by GDR were shown in **Figure S10**, which has similar trend with $MAPb_{0.6}Sn_{0.4}I_3$ by GDR method. This indicate our GDR method has large potential to be widely used in the synthesis of other Pb-Sn binary metal perovskites. To the best of our knowledge, this is the highest PCE demonstrated for all Pb-Sn PVSCs. The EQE spectrum with integrated photocurrent, stable out-put operation measurement and PCE statistics distribution in Figure **S8**, **S9** and **S10** prove our GRD strategy can be successfully extend to other perovskite systems.

Stability test

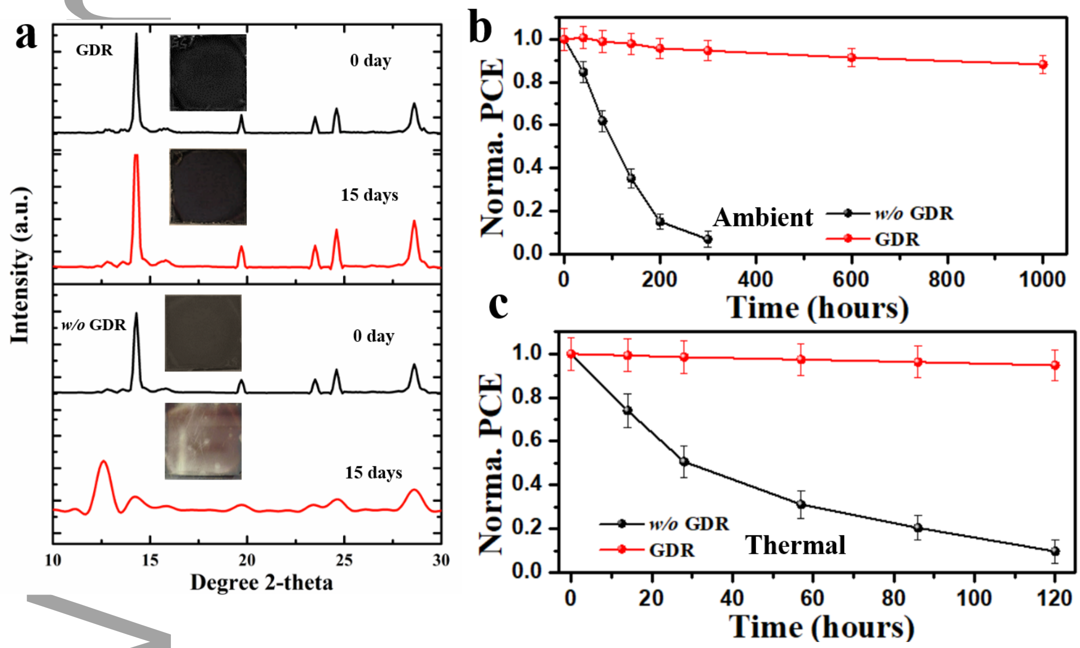

Figure 3 a) XRD pattern spectra and photographs of the reference and GDR-derived $MAPb_{0.6}Sn_{0.4}I_3$ films during the 15-days storage in ambient condition with a relative humidity of 40 ± 5%. **b)** Ambient and **c)** thermal stability test of the reference and GDR-derived $MAPb_{0.6}Sn_{0.4}I_3$ PVSCs as a function of storage time. Note that the ambient stability was recorded at room temperature with a 50-60% humidity and the thermal stability was traced under 80 ^{o}C in the ambient condition with a 50-60% humidity.

As the Sn incorporated PVSCs are notoriously prone to oxidation, we have carefully examined the stability of these Sn-containing PVSCs processed through the GDR approach. We first investigate the ambient stability of the perovskite films fabricated from the solution with or without GDR. All of the films were stored in air with a relative humidity of 40-50% at room temperature. Presented in **Figure 3a** are the XRD spectrum and real pictures of the degraded films. As can be seen, the reference $MAPb_{0.6}Sn_{0.4}I_3$ film totally decomposed into a yellow phase after being stored for 15 d whereas the $MAPb_{0.6}Sn_{0.4}I_3$ film prepared by the GDR-derived solution remained intact in black, showing much-improved ambient stability. The XRD patterns of those degraded films as a function of stored time in ambient unraveled the possible degradation pathways. Intense PbI_2 and SnI_2 peaks at ~ 12.5^o appeared in the reference $MAPb_{0.6}Sn_{0.4}I_3$ film after 15 d storage in ambient whereas they were absent in the GDR-derived $MAPb_{0.6}Sn_{0.4}I_3$ film after the same period of time and also over 40 days in ambient (shown in **Figure S11**).

Besides, the XRD peaks broadened in the reference $MAPb_{0.6}Sn_{0.4}I_3$ film, indicating its decreased crystallinity after aging. On the contrary, the GDR-derived $MAPb_{0.6}Sn_{0.4}I_3$ film showed retarded conversion into PbI_2 yellow phase after being stored in ambient for 15 d.

The ambient and thermal stability of the derived PVSCs were further examined and the initial efficiencies were from mean cell efficiencies in **Table S3**. As illustrated in **Figure 3b,** the PCE of the GDR-derived $MAPb_{0.6}Sn_{0.4}I_3$ PVSC retained over 90% of its initial PCE after being exposed to ambient air (40-50% relative humidity) for 1000 h but the reference device quickly decayed after only being exposed for 250 h. Moreover, the thermal stability of these fabricated devices was also examined as shown in **Figure 3c**. The GDR-derived $MAPb_{0.6}Sn_{0.4}I_3$ PVSC retained over 90% of its original PCE after being annealed at 80 °C in ambient for 120 h, however, the PCE of the reference $MAPb_{0.6}Sn_{0.4}I_3$ PVSC dropped to below 20% of its initial value. Other parameters including J_{SC}, V_{OC} and FF as the function of storage time under ambient or thermal aging were shown in **Figure S12** and **S113**. All these outstanding stability data highlight the advantages of preparing binary perovskites by the GDR approach. Moreover, shown in **Figure S14**, the GDR-derived

$(FAPb_{0.6}Sn_{0.4}I_3)_{0.85}(MAPb_{0.6}Sn_{0.4}Br_3)_{0.15}$ PVSC also obtained over 90% of its original PCE after being stored to ambient air (40-50% relative humidity) for 300 h or annealed at 80 °C in ambient for 100 h, indicating outstanding stability with the GDR method derived Pb-Sn binary perovskite.

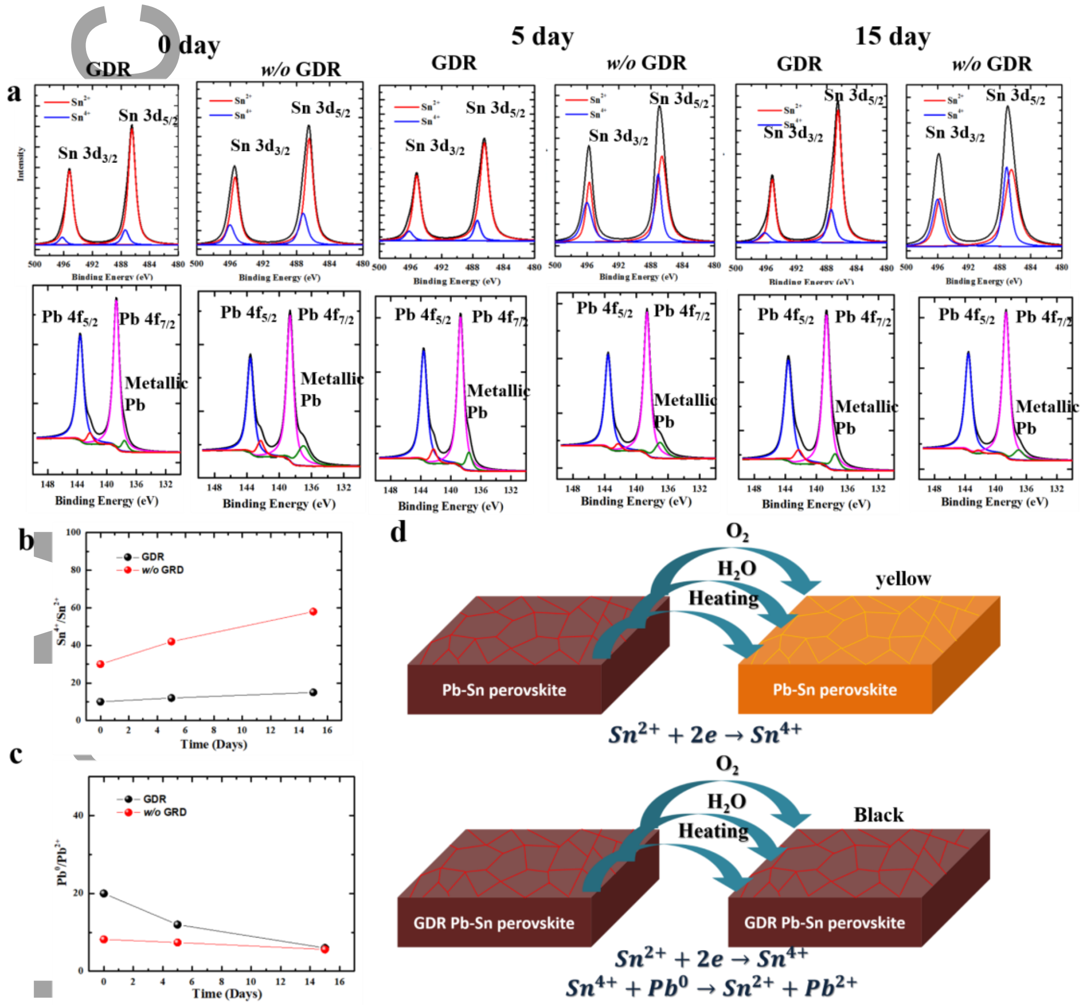

Figure 4 (a) XPS of the $MAPb_{0.6}Sn_{0.4}I_3$ films stored in ambient environment for 0 day (left), 5 days (middle), and 15 days (right). The obtained ratios of (b) Sn^{4+}/Sn^{2+} and (c) Pb^0/Pb^{2+} of the $MAPb_{0.6}Sn_{0.4}I_3$ films from the XPS spectra as a function of storage time. d) Schemes of the aged reference and GDR-derived $MAPb_{0.6}Sn_{0.4}I_3$ films.

To investigate the underlying mechanisms of the improved ambient stability in the GDR-derived $MAPb_{0.6}Sn_{0.4}I_3$ film, we have resorted to chemical state analysis and elemental analysis using XPS. **Figure 4a** presented the Sn states of the reference and GDR-derived $MAPb_{0.6}Sn_{0.4}I_3$ films. As shown, the Sn 3d peak in these films was deconvoluted into Sn^{4+} and Sn^{2+} ions, respectively, and the Sn^{4+}/Sn^{2+} ratio was calculated accordingly as illustrated in **Figure 4b**. As shown, the GDR-derived $MAPb_{0.6}Sn_{0.4}I_3$ possesses lower Sn^{4+}/Sn^{2+} ratio compared to the reference $MAPb_{0.6}Sn_{0.4}I_3$ film. This indicates that the film prepared by the GDR-derived solution possesses a lower degree of Sn^{2+} oxidation, which might play a pivotal role for the enhanced performance observed.

Figure 4a also presents the Pb states of the studied films, where two feature peaks of Pb $4f^{7/2}$ and Pb $4f^{5/2}$ were clearly observed. The Pb $4f^{7/2}$ core level comprises two deconvoluted peaks centered on ca. 137.9 and 136.3 eV. The more intense one is associated with the Pb^{2+}, while the other one is associated to metallic Pb^0, resulting from the decomposition of $MAPbI_3$.[35, 36] Surprisingly, the GDR-derived $MAPb_{0.6}Sn_{0.4}I_3$ film revealed a higher Pb^0/Pb^{2+} ratio than the reference film. This might be traced to the fact that more residual Pb^0 was formed in the GDR-derived solution according to Equation (d). We next compare the Sn^{4+}/Sn^{2+} and Pb^0/Pb^{2+} ratios of both films as a function of storage time as plotted in **Figure 4b-4c**. Taking the evidences revealed by device characteristics and XPS spectroscopy, we propose that the residual Pb^0 in GDR-derived film can further reduce the formed Sn^{4+} back to Sn^{2+} to enhance the film robustness against the oxidation portrayed in **Figure 4e**. As shown, the Sn^{4+}/Sn^{2+} ratio of the reference $MAPb_{0.6}Sn_{0.4}I_3$ film quickly raised after being exposed to air while the value of the GDR-derived $MAPb_{0.6}Sn_{0.4}I_3$ film remained almost the same. This clearly illustrates the advantage of GDR-derived film in inhibiting Sn^{2+} oxidization while being stored in ambient. Interestingly, the Pb^0/Pb^{2+} ratio of the GDR-derived film gradually reduced after being exposed to air while the value of the reference film only shows slight decrease.

Conclusion

We have demonstrated a simple and generally applicable approach in preparing stable Pb-Sn binary perovskite films via a galvanic displacement reaction (GDR). By tuning the reaction time, the $MAPb_xSn_{1-x}I_3$ films with different Pb/Sn ratios could be obtained to exhibt improved ambient stability. The PVSCs derived from these films showed a PCE of 15.76%. The GDR method can also be applicable to make other mixed perovskite compositions for PVSCs. The $(FAPb_{0.6}Sn_{0.4}I_3)_{0.85}(MAPb_{0.6}Sn_{0.4}Br_3)_{0.15}$ based PVSC showed a promising PCE of 18.21%, which is the highest PCE reported to date for PVSC based on the Pb-Sn binary perovskites. Benefiting from the improved stability of the perovskite films, the devices also exhibit much better ambient stability, which could retain > 90% of the initial PCE of device after being stored in ambient (RH~50%) for 1000 h. This work highlights the versatility of preparing binary metal halide perovskites, and could be generally applicable to a wide range of perovskites with mixed metal cations to further enhance performance and stability.

Methods

Materials All materials including MAI (98%), FAI (≥99%, anhydrous), MABr (98%), SnI_2 (anhydrous, beads, −10 mesh, 99.99% trace metals basis), PbI_2(99%), DMF (for HPLC, ≥99.9%), DMSO (99.7%), Sn powder (powder, -100 mesh, 99.99% trace metals basis) , PCBM (≥99.9%).were purchased from Sigma-Aldrich and used without further purification except notice.

Solution preparation The $MAPbI_3$ precursor solution was prepared by dissolving CH_3NH_3I (MAI) and PbI_2 with a molar ratio of 1 M:1.08 M in DMF and DMSO (volume ratio of 4:1). The reference $MAPb_xSn_{1-x}I_3$ was prepared with similar method, except different ratio of PbI_2/SnI_2, the total molar desnisty of PbI_2 and SnI_2 is 1.08 M. The $[HC(NH_2)_2]_{0.85}[CH_3NH_3]_{0.15}Pb[I_{0.85}Br_{0.15}]_3$ solution was prepared by mixing $HC(NH_2)_2I$ (FAI), (PbI_2, CH_3NH_3Br (MABr), and $PbBr_2$ in a co-solvent of DMF and DMSO (volume ratio 4:1) with the molar concentration of 1.35M Pb^{2+} (PbI_2 and $PbBr_2$, The molar ratio of $PbI_2/PbBr_2$=85/15, PbI_2/FAI=1.05, $PbBr_2$/MABr=1/1).

The GDR-based perovksite solution was prepared by mixing solid Sn powders into the prepared Pb based perovskite solutions with a molar ratio of 3:1 between Sn^{2+} and Pb^{2+}. Normally, the solution was keeped and stirred at 70 °C. The Sn^{2+} concentration would increase with the reaction time. For the typical $MAPb_{0.6}Sn_{0.4}I_3$, the solution was heated and stirred at 70 °C for 3 d. The mixed solution was filtered with a 0.45 µm PTFE filter before use.

As reported previously, 15 mg $PC_{61}BM$ was dissolved into 1 mL chloroform and bis-C60 solution was prepared by dissolving 2 mg bis-C_{60} into 1 mL IPA, followed by sonication for 1 h.[37]

Photovoltaic device fabrication and characterization ITO glass (15 Ω sq^{-1}) was cleaned through sequential sonication with deionized water, acetone, and isopropyl alcohol for 20 min, respectively. The cleaned ITO substrates were then treated by UV ozone for 15 min before use. The PEDOT:PSS (Baytron 4083) was spin-coated onto ITO substrates at 4000 rpm for 30 s. Then after heating at 150 °C for 10 min. The perovskite precursor solution was then spin-coated onto the above prepared films at 1000 rpm 10s and 5000 rpm for 30 s. During the last 10 s of the second spin-coating step, the substrate was treated with chlorobenzene drop-casting (0.1 mL). The as spun films were annealed at 100 °C for 10 min. Then, the PCBM electron-transporting layer was deposited by spin-coating at 1500 rpm for 60 s and 2000 rpm for 5 s. Afterward, the surfactant layer bis-C60 was spin-coated at 3000 rpm for 30 s. Finally, a 120 nm thick top Ag electrode was evaporated under high vacuum (< 1×10^{-6} Torr). A typical active device area is defined by a metal mask with an aperture are of 5.9 mm^2 aligned with the device area when under illumination test. All cells were encapsulated using epoxy inside the glovebox.

Characterization Device *J–V* characteristics were measured under the AM1.5G (100 mW cm^{-2}) condition using a Newport solar simulator in air at room temperature. A standard Si diode with KG5 filter was purchased from PV Measurements and calibrated by Newport Corporation. The light intensity was calibrated using the Si diode as a reference cell to bring the spectral mismatch to unity. *J–V* characteristics were recorded using a Keithley 2400 source meter unit. EQEs were characterized using an Enlitech QE-S EQE system equipped with a standard Si diode, and monochromatic light was generated from a Newport 300W lamp source. The stable output PCE, was measured by setting the bias voltage around the maximum power-point and then tracing the current density. The bias voltage at maximum power point was determined from the J-V curve. The stability test was carried on by storing at ambient environment (25 °C and 40-60% humidity). SEM images and EDX mapping were obtained from JEOL 7100F operated at 5 kV and 10 kV respectively. X-ray diffraction (XRD) patterns of the samples were done by Philips PW 1830 with Cu Ka radiation. UV–vis absorption spectra were recorded on a Perkin–Elmer UV–vis spectrophotometer (model Lambda 20). For steady-state PL, a 514.5 nm ultrafast laser was used as the excitation light source (Laser sources: Ar ion laser, 50 mW). The absorption spectra were measured by Varian Cary 5000 UV-Vis-NIR. Time-resolved photoluminescence (TRPL) was measured with a 470 nm pulsed laser generated from the second-harmonic generation to excite the samples with a time-correlated single photon counting (TCSPC) system and the PL lifetime was fitted with a one-exponential function. XPS was carried out by a Kratos Axis Ultra DLD multi-technique surface analysis system using monochromatized Al Kα X–ray photons (hν = 1486.6 eV) at a pass energy of 20 eV and energy resolution of 800 meV. For the peak fitting, the data of XPS peaks were fitted by XPS Peak 3.0 Fitting software. For the presented lead and tin peaks, a Shirley background was subtracted. The peak position for the Sn and Pb with different valence was initially selected according to previous reports.[38-40] The peak type for Sn and Pb was d and f, respectively. By optimizing the Gaussian-Lorentzian (G/L) ratio, the final peak position, full-width-half-maximum (FWHM), peak area would be calculated by the fitting program.

Acknowledgments

We thank Prof. Chu-Chen Chueh for the manuscript discussion and revision. This work was supported by the National Science Foundation (DMR-1608279), the Office of Naval Research (N00014-17-1-2260), the Asian Office of Aerospace R&D (FA2386-15-1-4106), and the Department of Energy SunShot (DE-EE 0006710). It was also funded by the National Natural Science Foundation of China under Grant Nos. 51273104 and 91433205. Dr. Zhu thanks the support of New Faculty Start-up Grant of the City University of Hong Kong (9610421, 7200587)

Contributions

Z. Z. and A. K.-Y. J. conceived the experiments. A. K.-Y. J. supervised the project. Z. Z. and N. L. designed the experiments. Z. Z., N. L., D. Z., conducted the experiments. Z.Z. wrote the original manuscript, and all authors revised it and commented on the final paper.

Competing interests

The authors declare that they have no competing interests.

Reference

1. M. A. Green, A. Ho-Baillie and H. J. Snaith, *Nat. Photonics*, 2014, **8**, 506-514.

2. T. M. Brenner, D. A. Egger, L. Kronik, G. Hodes and D. Cahen, *Nat. Rev. Mater.*, 2016, **1**, 15007.

3. S. D. Stranks and H. J. Snaith, *Nat. Nanotechnol.*, 2015, **10**, 391-402.

4. J.-P. Correa-Baena, T. Buonassisi, J.-P. Correa-Baena, M. Saliba, M. Gratzel, W. Tress, A. Hagfeldt and A. Abate, *Science*, 2017, **358**, 739-744.

5. NREL chart, 2018, https://www.nrel.gov/pv/assets/images/efficiency-chart-20180716.jpg

6. F. Hao, C. C. Stoumpos, R. P. H. Chang and M. G. Kanatzidis, *J. Am. Chem. Soc.*, 2014, **136**, 8094-8099.

7. F. Zuo, S. T. Williams, P.-W. Liang, C.-C. Chueh, C.-Y. Liao and A. K. Y. Jen, *Adv. Mater.*, 2014, **26**, 6454-6460.

8. W. Liao, D. Zhao, Y. Yu, N. Shrestha, K. Ghimire, C. R. Grice, C. Wang, Y. Xiao, A. J. Cimaroli, R. J. Ellingson, N. J. Podraza, K. Zhu, R.-G. Xiong and Y. Yan, *J. Am. Chem. Soc.*, 2016, **138**, 12360-12363.

9. D. Zhao, Y. Yu, C. Wang, W. Liao, N. Shrestha, C. R. Grice, A. J. Cimaroli, L. Guan, R. J. Ellingson, K. Zhu, X. Zhao, R.-G. Xiong and Y. Yan, *Nat. Energy*, 2017, **2**, 17018.

10. Z. Yang, A. Rajagopal, C.-C. Chueh, S. B. Jo, B. Liu, T. Zhao and A. K. Y. Jen, *Adv. Mater.*, 2016, **28**, 8990-8997.

11. G. E. Eperon, T. Leijtens, K. A. Bush, R. Prasanna, T. Green, J. T.-W. Wang, D. P. McMeekin, G. Volonakis, R. L. Milot, R. May, A. Palmstrom, D. J. Slotcavage, R. A. Belisle, J. B. Patel, E. S. Parrott, R. J. Sutton, W. Ma, F. Moghadam, B. Conings, A. Babayigit, H.-G. Boyen, S. Bent, F. Giustino, L. M. Herz, M. B. Johnston, M. D. McGehee and H. J. Snaith, *Science*, 2016, DOI: 10.1126/science.aaf9717, aaf9717.

12. Z. Yang, A. Rajagopal and A. K. Y. Jen, *Adv. Mater.*, 2017, **29**, 1704418.

13. D. Zhao, C. Wang, Z. Song, Y. Yu, C. Chen, X. Zhao, K. Zhu and Y. Yan, *ACS Energy Lett.*, 2018, **3**, 305-306.

14. A. Rajagopal, Z. Yang, S. B. Jo, I. L. Braly, P.-W. Liang, H. W. Hillhouse and A. K. Y. Jen, *Adv. Mater.* , 2017, **29**, 1702140.

15. T. Leijtens, R. Prasanna, A. Gold-Parker, M. F. Toney and M. D. McGehee, *ACS Energy Lett.*, 2017, **2**, 2159-2165.

16. F. Gu, S. Ye, Z. Zhao, H. Rao, Z. Liu, Z. Bian and C. Huang, *Solar RRL*, 2018, **2**, 1800136.

17. F. Hao, C. C. Stoumpos, D. H. Cao, R. P. H. Chang and M. G. Kanatzidis, *Nat. Photonics*, 2014, **8**, 489.

18. W. Ke, C. C. Stoumpos, M. Zhu, L. Mao, I. Spanopoulos, J. Liu, O. Y. Kontsevoi, M. Chen, D. Sarma, Y. Zhang, M. R. Wasielewski and M. G. Kanatzidis, *Sci. Adv.*, 2017, **3**.

19. M. Konstantakou and T. Stergiopoulos, *J. Mater. Chem. A*, 2017, **5**, 11518-11549.

20. Y. Zhou, Z. Zhou, M. Chen, Y. Zong, J. Huang, S. Pang and N. P. Padture, *J. Mater. Chem. A*, 2016, **4**, 17623-17635.

21. S. J. Lee, S. S. Shin, Y. C. Kim, D. Kim, T. K. Ahn, J. H. Noh, J. Seo and S. I. Seok, *J. Am. Chem. Soc.*, 2016, **138**, 3974-3977.

22. T. M. Koh, T. Krishnamoorthy, N. Yantara, C. Shi, W. L. Leong, P. P. Boix, A. C. Grimsdale, S. G. Mhaisalkar and N. Mathews, *J. Mater. Chem. A*, 2015, **3**, 14996-15000.

23. I. Chung, B. Lee, J. He, R. P. H. Chang and M. G. Kanatzidis, *Nature*, 2012, **485**, 486.

24. Z. Zhu, C.-C. Chueh, N. Li, C. Mao and A. K. Y. Jen, *Adv. Mater.*, 2018, **30**, 1703800-n/a.

25. Y. Liao, H. Liu, W. Zhou, D. Yang, Y. Shang, Z. Shi, B. Li, X. Jiang, L. Zhang, L. N. Quan, R. Quintero-Bermudez, B. R. Sutherland, Q. Mi, E. H. Sargent and Z. Ning, *J. Am. Chem. Soc.*, 2017, **139**, 6693-6699.

26. S. Shao, J. Liu, G. Portale, H.-H. Fang, G. R. Blake, G. H. ten Brink, L. J. A. Koster and M. A. Loi, *Adv. Energy Mater.*, 2018, **8**, 1702019.

27. Barke, Hans-Dieter; Hazari, Al; Yitbarek, Sileshi (2008). Misconceptions in chemistry addressing perceptions in chemical education (Online-Ausg. ed.). Berlin: Springer. pp. 227–228. ISBN 3540709894.

28. X. Xia, Y. Wang, A. Ruditskiy and Y. Xia, *Adv. Mater.*, 2013, **25**, 6313-6333.

29. K. An and T. Hyeon, *Nano Today*, 2009, **4**, 359-373.

30. C. M. Cobley and Y. Xia, *Mater. Sci. Eng. R Rep.*, 2010, **70**, 44-62.

31. Vanýsek, Petr (2012). "Electrochemical Series". In Haynes, William M. Handbook of Chemistry and Physics: 93rd Edition. Chemical Rubber Company. pp. 5–80. ISBN 9781439880494..

32. X. Xu, C.-C. Chueh, Z. Yang, A. Rajagopal, J. Xu, S. B. Jo and A. K. Y. Jen, *Nano Energy*, 2017, **34**, 392-398.

33. Y. Li, W. Sun, W. Yan, S. Ye, H. Rao, H. Peng, Z. Zhao, Z. Bian, Z. Liu, H. Zhou and C. Huang, *Adv. Energy Mater.*, 2016, **6**, 1601353.

34. J. Im, C. C. Stoumpos, H. Jin, A. J. Freeman and M. G. Kanatzidis, *J. Phys. Chem. Lett.*, 2015, **6**, 3503-3509.

35. Y. Li, X. Xu, C. Wang, B. Ecker, J. Yang, J. Huang and Y. Gao, *J. Phys. Chem. C*, 2017, **121**, 3904-3910.

36. S. Wang, Y. Jiang, Emilio J. Juarez-Perez, Luis K. Ono and Y. Qi, *Nat. Energy*, 2016, **2**, 16195.

37. N. Li, Z. Zhu, C.-C. Chueh, H. Liu, B. Peng, A. Petrone, X. Li, L. Wang and A. K.-Y. Jen, *Adv. Energy Mater.*, 2017, **7**, 1601307.

38. B. Conings, L. Baeten, C. De Dobbelaere, J. D'Haen, J. Manca and H.-G. Boyen, *Adv. Mater.*, 2014, **26**, 2041-2046.

39. S. R. Raga, M.-C. Jung, M. V. Lee, M. R. Leyden, Y. Kato and Y. Qi, *Chem. Mater.*, 2015, **27**, 1597-1603.

40. W. Li, J. Li, J. Li, J. Fan, Y. Mai and L. Wang, *J. Mater. Chem. A*, 2016, **4**, 17104-17110.

We demonstrate a simple and generally applicable method to fabricate efficient and stable Pb-Sn binary perovskite solar cells (PVSCs) based on a galvanic displacement reaction (GDR). With optimizing the ration of Pb and Sn, high PCEs of 15.85% and 18.21% has be achieved for Pb-Sn binary based PVSCs. Moreover, these Pb-Sn based PVSCs exhibit improved ambient and thermal stability with encapsulation.

Keyword: Galvanic Displacement Reaction, Pb/Sn Binary Perovskite, Solar Cells

Zonglong Zhu,[1,2†] Nan Li,[1,3†] Dongbin Zhao,[1,4] Liduo Wang,[3] and Alex K.-Y. Jen[1,2,5*]

Improved Efficiency and Stability of Pb/Sn Binary Perovskite Solar Cells Fabricated by Galvanic Displacement Reaction